

Spinodal decomposition in a two-dimensional fluid model

James E. Farrell

School of Physics and Astronomy, University of Minnesota, Minneapolis, Minnesota 55455

Oriol T. Valls

School of Physics and Astronomy and Minnesota Supercomputer Institute, University of Minnesota, Minneapolis, Minnesota 55455

(Received 24 April 1989)

Spinodal decomposition after a deep quench is studied numerically through the use of a Langevin fluid model containing a conserved scalar order parameter and a conserved current. The couplings involving the order parameter and the currents are as in the standard model *H* (in the taxonomy of Hohenberg and Halperin), which becomes model *B* in the limit where current and order parameter decouple. In this model, the late scaling-regime domain growth is faster not only than in model *B*, but also than in a Langevin fluid model with couplings to pressure fluctuations only. In the intermediate-time regime, the behavior observed is similar to that of model *B*. A crossover to the faster dynamics occurs subsequently. The exponent n for the domain growth law $l(t) \sim t^n$ is found to be $n = 0.69 \pm 0.02$ at the longest times considered. The order-parameter correlations and their scaling behavior are studied. The current correlations are shown to equilibrate rather quickly. Our results put in doubt the idea of a "universality class" for nonequilibrium fluid models.

I. INTRODUCTION

Spinodal decomposition (SD) is an archetypical non-equilibrium growth process occurring after a system is placed into an unstable region of its phase diagram usually by means of a rapid temperature or pressure quench.¹ It occurs in, among other systems, solid or liquid mixtures quenched below the miscibility gap, leading to separation of the two components, and also in fluids quenched into the liquid-gas coexistence region. SD is the process of phase separation characterized by a spontaneous formation of domains which then proceed to grow and combine. This spontaneous formation requires no activation energy to initiate the separation and therefore does not depend upon initial large fluctuations in the order parameter to begin the ordering process.

SD has been experimentally studied extensively both in binary alloys^{2,3} and in fluid systems.^{4,5} After the initial nucleation of domains, their growth as a function of time is typically characterized by a power law; if $l(t)$ is a linear measure of domain size, then $l(t) \sim t^n$, where n is known as the growth exponent. The reported values of n are sometimes themselves time dependent. Much emphasis has been placed into classifying order growth phenomena into "universality classes"⁶ according to the ultimate value of the exponent n for "asymptotically long" times. Experimental studies of binary fluid systems subjected to deep temperature or pressure quenches^{4,5} have revealed several distinct time regimes and exponents, among which are an early-time power-law growth, where a rather small growth exponent $n \approx 0.3$ or 0.4 is observed, and a late-time regime in which $n \approx 1$. Experiments on binary alloys measure much smaller exponents (e.g., $n \approx 0.2$ in Ref. 3). It seems physically obvious that domains can grow faster in fluids because of the freely flowing matter allowing similar fluid molecules to congregate and permitting the speedy combination of nascent

domains. While there is a wealth of SD experiments in fluid systems, with the exception of one isolated study⁷ there has been little effort to better understand SD in fluid-type models through numerical studies.

Analytical work on SD in fluids has been inconclusive to date, but many compelling questions have been raised. Siggia⁸ predicted for binary fluids $n = \frac{1}{3}$ in the early stages of the growth process changing to $n = 1$ asymptotically. This is compatible with many of the experimental results for quenches far from metastability and far from the critical region.^{4,5} To predict the growth in the late-time regime, Siggia showed that tubular domain structures of one of the phases were unstable to surface fluctuations and would grow with the exponent $n = 1$. In Ref. 9 it was pointed out that Siggia's derivation might not be applicable to two-dimensional fluids and, relying upon a particular approximation to hydrodynamics, rather different growth dynamics were predicted for that case: $n = \frac{1}{2}$ for both the early- and late-time regimes. This prediction was confirmed in a numerical study of a stochastic Langevin model of a two-dimensional fluid performed in Ref. 7 where an exponent $n = \frac{1}{2}$ was also obtained. This value is clearly larger than the value^{10,11} $n \approx 0.3$ which one obtains for the standard model (model *B* in the taxonomy of Halperin and Hohenberg¹²) of spinodal decomposition in a system with a scalar, conserved order parameter and no currents.¹³ Thus the relevance of currents is well established.

In this work we will explore further the influence of currents upon SD in fluids by studying a very important stochastic model of fluid behavior. Because of the complexity of models which would properly account for the effects of currents, there has been only one simulation of SD with scalar order-parameter field coupled to a current vector field. One of the issues we are attempting to resolve about the role that currents play in SD is whether the growth kinetics depend on the specific set of cou-

plings between the fields. The linearized version of the models studied numerically in Ref. 7 and analytically in Ref. 9 includes sound modes but not thermal diffusion. We therefore choose to study here another stochastic model in which the couplings are chosen in such a way as to maintain thermal diffusion modes and current dissipation (e.g., model H of Ref. 12). This model allows us to tackle some important universality problems. It is well known¹² that the dynamical critical exponents for fluids are correctly predicted by model H rather than by a model such as that studied in Ref. 7. It is therefore, *a priori*, at least conceivable that the two types of dynamics also have different properties with regard to growth kinetics. Further, this model can be reduced to model B by turning off the coupling parameter to the current, which cannot be done for the model studied in Ref. 7. We can therefore directly investigate the influence of the currents. We will see that our results indicate a breakdown of universality: we obtain an exponent n larger than $\frac{1}{2}$ and *a fortiori* larger than that of model B .

After this introduction we will present in Sec. II a review of the derivation of the precise model employed in this work and a discussion of the dimensionless variables used there. In Sec. III, we will discuss the methods of our numerical solution performed on a two-dimensional square lattice for a deep quench through the critical point. Initial conditions and the temperature quench will be discussed. The particular choice of parameters will be justified as will the lattice size and time scales over which we evolved our system of equations. In Sec. IV we will present our results. We will analyze the process of current equilibration through the current-current correlation functions. The ordering and growth of domains characterized by the values of the order-parameter correlations will be measured and analyzed in two different ways. The results of these two methods will be compared and scaling properties of the growth process will be discussed. Our results are contrasted with those obtained for other two-dimensional fluid models.

II. THE MODEL

A very important physical difference between spinodal decomposition in fluids and in alloys is the existence of convective phenomena in the former, which requires the inclusion of currents in the model studied. Physical phenomena such as diffusion of heat and free convective flows must be modeled in a fluid system having a two-phase region if we hope to calculate the correct growth dynamics. The proper couplings involving the scalar field variable and the vector current will be included to ensure that the desired hydrodynamics are present in this model as explained in the Introduction.

Langevin equation models represent only an approximation to the actual behavior of fluids. The question of developing quantitatively realistic and yet relatively simple models to describe fluids received a great deal of attention years ago in the context of the calculation of dynamical critical exponents (see Ref. 12 for a review). It was found that for critical dynamics calculations, a model with a single scalar density coupled to one current and

including heat transport modes and no pressure fluctuations in its linearized form was sufficient. This is the model denoted as “model H ” in Ref. 12.

While one cannot regard it as being necessarily true, much less as proved, that what is best for second-order transitions is also best for first-order ones, inclusion of heat or entropy transport might be crucial to the process of spinodal decomposition. It is clearly of great interest to examine the behavior of models with dynamics of the H type, and by comparing with the results of Ref. 7, to determine whether the presence of heat diffusion versus pressure fluctuations is indeed relevant in SD. For instance, we would like to determine the effect of these different types of dynamics on the growth exponent n governing the growth of domain size $l(t)$ by the power-law relation $l(t) \sim t^n$. We have therefore chosen to study a version of model H in this paper. Model H was originally derived by Kawasaki¹⁴ and co-workers and, as has been explained above, has been found to be extremely successful as a model of the second order phase transition in binary fluids and liquid-gas systems.

As a first step in reviewing the derivation of the model equations we recall some elementary aspects of the Langevin formulation. The Langevin equations are a system of coupled differential equations involving a set of coarse grained variables $[\varphi_\alpha]$. To choose the correct set of coarse grained variables appropriate to a fluid system, one should start with the equations of hydrodynamics,¹⁵ which are $2+d$ coupled equations involving $4+d$ variables (entropy, density, pressure, temperature, and momentum density) in the fluid system; d is the spatial dimension of the system. In a binary fluid system, an additional variable, namely, the concentration, and an additional concentration continuity equation would also be included. Two of the scalar variables may be written in terms of the remaining two independent variables through the use of thermodynamic relations; the choice of the independent scalar variables to keep is rather arbitrary. In model H only one scalar variable is kept;¹⁶ in decoupling the sound modes from the heat modes, one of the scalar densities is made a nonfluctuating constant. Thus the set $[\varphi]$ we consider here will consist of the scalar density ψ and the vector momentum density \mathbf{g} : $[\varphi_\alpha] = [\psi, \mathbf{g}]$.

First, we consider briefly the equilibrium state. The equilibrium properties of our model are given in terms of a free-energy functional $F[\varphi_\alpha]$. The equilibrium averages $\langle A \rangle_{\text{eq}}$ of some observable A are determined in the following way:

$$\langle A \rangle_{\text{eq}} = \frac{1}{Z} \int \exp(-\beta F[\varphi_\alpha]) A[\varphi_\alpha] d[\varphi_\alpha], \quad (2.1)$$

where $\beta = 1/T$, the Boltzmann constant being taken to be unity in the units used here, $F[\varphi]$ is the free-energy functional, and Z is the normalization $Z = \int \exp(-\beta F[\varphi_\alpha]) d[\varphi_\alpha]$; the integral is a functional integral. The equilibrium properties that we need to model properly include the current-current correlations obeying the equipartition theorem, the presence of ordered domains, and the characteristics of the domain

walls separating the different fluid components. For the liquid-gas transition or for most binary fluid demixing transitions, the coexistence curve in the phase diagram is asymmetric. In general, the free energy at a temperature far from the critical temperature T_c should be asymmetric upon change of sign of the order parameter. However, the symmetric double-well free energy that we will choose for SD is the same as was used to successfully model the critical behavior of fluids. This free energy is of the form

$$F[\psi, \mathbf{g}] = \frac{1}{2} \int d^d \mathbf{r} \left[\frac{1}{\rho_0} \mathbf{g}^2(\mathbf{r}) + u \psi^4(\mathbf{r}) - r \psi^2(\mathbf{r}) + K' |\nabla \psi(\mathbf{r})|^2 \right], \quad (2.2)$$

where the first term is the kinetic energy contribution and the remaining terms are a Ginzburg-Landau expansion of the free energy in powers of the order parameter. The variable r is positive below T_c . This expansion is the simplest free energy one can use to model a symmetry breaking phase transition. It is valid both for small ψ : there are no terms of higher order than ψ^4 , and for slowly varying ψ : there are no terms of higher derivative than the $|\nabla \psi(\mathbf{r})|^2$. This free energy is minimized when ψ falls into the $\psi = \pm(r/u)^{1/2}$ wells and is also reduced by lowering the surface energy associated with the domain walls which separate the positive ψ and negative ψ domains. Note that ρ_0 is the average mass density. The absence of mass density fluctuations in the kinetic energy term is in contrast to the model studied in Ref. 7.

We now review the highlights of the derivation of the dynamical equations of the model studied here. We start from the generalized Langevin equation which is written as follows:

$$\partial_t \varphi_\alpha(\mathbf{r}, t) = \sum_\beta \Gamma_{\alpha\beta} \frac{\delta F[\varphi]}{\delta \varphi_\beta(\mathbf{r}, t)} + V_\alpha[\varphi] + \eta_\alpha(\mathbf{r}, t), \quad (2.3)$$

where the first term on the right is a set of dissipative terms, e.g., thermal diffusion and viscous drag effects. The $\Gamma_{\alpha\beta}$ operator determines the form of the dissipation in this system. If this operator were merely a constant, the variables would not be conserved. The $\eta_\alpha(\mathbf{r}, t)$ are Gaussian noise terms which account for the effects on the coarse grained variables of all the quickly fluctuating variables which are not explicitly monitored. The $V_\alpha[\varphi]$ are the streaming velocities which are nonlinear, deterministic, mode coupling terms, e.g., the additional term in the convective derivative. The streaming velocities are calculated from the Poisson brackets as follows:¹⁷

$$V_\alpha[\varphi] = \sum_{\mathbf{r}', \beta} \left[\frac{\delta}{\delta \varphi_\beta(\mathbf{r}', t)} Q_{\alpha\beta}(\mathbf{r}, \mathbf{r}') - Q_{\alpha\beta}(\mathbf{r}, \mathbf{r}') \frac{\delta F[\varphi]}{\delta \varphi_\beta(\mathbf{r}, t)} \right], \quad (2.4)$$

where

$$Q_{\alpha\beta}(\mathbf{r}, \mathbf{r}') = \lambda_{\alpha\beta} \{ \varphi_\alpha(\mathbf{r}, t), \varphi_\beta(\mathbf{r}', t) \}, \quad (2.5)$$

the braces signify Poisson brackets and $\lambda_{\alpha\beta}$ is a symmetric matrix of coupling coefficients. These streaming

velocities will account for the nonlinear part of the effects due to collective mass flows.

The correlation functions for the noise sources in (2.3) are determined from the fluctuation-dissipation theorem and they are as follows:

$$\langle \eta_\alpha(\mathbf{r}, t) \eta_\beta(\mathbf{r}', t') \rangle = -2T \Gamma_{\alpha\beta} \delta^d(\mathbf{r} - \mathbf{r}') \delta(t - t'), \quad (2.6)$$

where T is the temperature and the $\Gamma_{\alpha\beta}$ operators were introduced in (2.3). Note that these noise sources are taken to be completely uncorrelated except at the same time and the same coordinate. Any possible cross correlations between noise sources are determined by the off-diagonal elements in $\Gamma_{\alpha\beta}$. The strengths of these noise correlations are proportional to the temperature. The rate of equilibrium of the velocity field can be easily monitored by comparing the velocity correlation functions with the temperature by means of the equipartition theorem:

$$\langle g_i(\mathbf{r}, t) g_k(\mathbf{r}', t') \rangle = T \rho_0 \delta_{ik} \delta^d(\mathbf{r} - \mathbf{r}') \delta(t - t'), \quad (2.7)$$

which must be satisfied at late times when the system approaches equilibrium insofar as the conservation laws allow. The i, k indices indicate Cartesian components of the momentum density.

Our first task then is the calculation of the streaming velocities as prescribed above. For the set of variables $[\varphi_\alpha] = [\psi, \mathbf{g}]$ the required Poisson brackets are

$$\{g_i(\mathbf{r}), g_j(\mathbf{r}')\} = -g_i(\mathbf{r}') \nabla_j \delta^d(\mathbf{r} - \mathbf{r}') + g_j(\mathbf{r}) \nabla_i' \delta^d(\mathbf{r}' - \mathbf{r}), \quad (2.8)$$

$$\{g_i(\mathbf{r}), \psi(\mathbf{r}')\} = \psi(\mathbf{r}') \nabla_i' \delta^d(\mathbf{r}' - \mathbf{r}), \quad (2.9)$$

where ∇' indicates that the gradient operators only on the primed coordinates. Using these Poisson brackets we calculate the streaming velocities:

$$V_{g_i} = \lambda \psi(\mathbf{r}) \nabla_i \frac{\delta F}{\delta \psi(\mathbf{r})} + \xi \sum_k \left[\nabla_k \left[g_i(\mathbf{r}) \frac{\delta F}{\delta g_k(\mathbf{r})} \right] + g_k(\mathbf{r}) \nabla_i \frac{\delta F}{\delta g_k(\mathbf{r})} \right], \quad (2.10)$$

$$V_\psi = \sigma \nabla \cdot \left[\psi(\mathbf{r}) \frac{\delta F}{\delta \mathbf{g}(\mathbf{r})} \right]. \quad (2.11)$$

The constants λ , ξ , and σ are the nonvanishing coupling parameters $\lambda_{\alpha\beta}$ for this model. Couplings to pressure fluctuations have been dropped. Following standard procedure,¹² we take all of these coupling parameters to be equivalent, $\sigma = \xi = \lambda$. Therefore, only one parameter λ couples the equations for the various field variables. The free energy used in the above equations is given by (2.2).

Finally, we require the matrix $\Gamma_{\alpha\beta}$ which appears in the right-hand sides of (2.3) and (2.6). Since to our knowledge there is no information on the behavior of these dissipative operators very far from equilibrium, we simply choose them as given in linearized hydrodynamics, as was done in the study of critical exponents. A straightforward comparison between the linearized version of this model and linear hydrodynamics shows that

the only nonzero matrix elements are

$$\Gamma_{\psi\psi} = \Gamma \nabla^2, \quad (2.12)$$

$$\Gamma_{g_i g_k} = \eta \delta_{ik} \nabla^2 + [\eta(1-2/d) + \zeta] \nabla_i \nabla_k \equiv L_{ik}, \quad (2.13)$$

where η and ζ are the bare viscosities while Γ is the product of the bare heat diffusion coefficient and the constant

$$\partial_t \psi(\mathbf{r}, t) = \Gamma \nabla^2 \frac{\delta F}{\delta \psi(\mathbf{r}, t)} - \lambda \nabla \cdot \left[\psi(\mathbf{r}, t) \frac{\delta F}{\delta \mathbf{g}(\mathbf{r}, t)} \right] + \mu(\mathbf{r}, t), \quad (2.14)$$

$$\begin{aligned} \partial_t g_i(\mathbf{r}, t) = & \eta \nabla^2 \frac{\delta F}{\delta g_i(\mathbf{r}, t)} + \sum_k \sigma \nabla_i \nabla_k \frac{\delta F}{\delta g_k(\mathbf{r}, t)} - \lambda \psi(\mathbf{r}, t) \nabla_i \frac{\delta F}{\delta \psi(\mathbf{r}, t)} \\ & - \lambda \sum_k \left[\nabla_k \left[g_i(\mathbf{r}, t) \frac{\delta F}{\delta g_k(\mathbf{r}, t)} \right] + g_k(\mathbf{r}, t) \nabla_i \frac{\delta F}{\delta g_k(\mathbf{r}, t)} \right] + \nu_i(\mathbf{r}, t), \end{aligned} \quad (2.15)$$

where $\sigma = \eta(1-2/d) + \zeta$. The Gaussian noise fields in these equations are correlated as follows:

$$\langle (\mu(\mathbf{r}, t) \mu(\mathbf{r}', t')) \rangle = -2T \Gamma \nabla^2 \delta^d(\mathbf{r} - \mathbf{r}') \delta(t - t'), \quad (2.16)$$

$$\langle (\nu_i(\mathbf{r}, t) \nu_k(\mathbf{r}', t')) \rangle = -2TL_{ij} \delta^d(\mathbf{r} - \mathbf{r}') \delta(t - t'), \quad (2.17)$$

and L_{ik} is defined in (2.13). While the variables used here are coarse grained, the form of the equations is reassuringly similar to ordinary hydrodynamics. The first term on the right of (2.14) is the heat diffusion term, while the second term includes the convective derivative from hydrodynamics. The first two terms on the right of (2.15) are the viscous drag terms from the Navier-Stokes equation, and the convective derivative and additional nonlinear coupling terms follow the summation.

The above equations, as written, would lead directly to the standard form of the model H equations^{12,14} if one were to drop some of the nonlinear convective terms and make the additional assumption of setting $\nabla \cdot \mathbf{g} = 0$. We will keep all nonlinear terms and refrain from making this additional assumption.¹⁸ The latter would lead to considerable simplification in analytic calculations but would have the opposite effect in numerical work such as performed here. Of course, $\nabla \cdot \mathbf{g}$ is related through a conservation law to the mass density fluctuations whose coupling back to ψ and \mathbf{g} is neglected in the model as studied here.

Equations (2.14) and (2.15) as they now stand have ex-

1/ r in the free-energy expansion.

Now we are ready to write the Langevin equations for this particular model. By putting the above streaming velocities and the dissipative terms derived through the use of linearized hydrodynamics into the Langevin equations we get the following set of coupled differential equations with which we wish to study SD in fluids:

PLICITLY four parameters: the diffusion constant Γ , the viscosities η and ζ , and the coupling parameter λ . In addition, from the noise correlation relations, we have the temperature T , and in the free-energy functional $F[\psi, \mathbf{g}]$, the parameters ρ_0 , r , u , and K' . The number of parameters can be reduced without loss of generality by rescaling the variables ψ and \mathbf{g} , and making dimensionless the time and length scales. The rescaled field variables are given below in terms of the original variables,

$$\phi = \left[\frac{u}{r} \right]^{1/2} \psi, \quad (2.18)$$

$$\mathbf{j} = \left[\frac{1}{(\rho_0 K')} \right]^{1/2} \mathbf{g}, \quad (2.19)$$

where $K = (r/u)K'$. Putting these rescaled field variables into (2.2), we get the form for the rescaled free energy \hat{F} ,

$$F[\varphi, \mathbf{j}] = \frac{K}{2} \int d^d r [\theta(\varphi^4 - \varphi^2) + |\nabla \varphi|^2 + |\mathbf{j}|^2] \equiv K \hat{F}[\varphi, \mathbf{j}], \quad (2.20)$$

where $\theta = r/K'$ is the quantity that gives the relative depth of the wells in the free-energy functional as compared to the energy needed to form domain walls. The coupled differential equations are simplified with the substitution of the rescaled dynamical variables and dimensionless free energy to the form,

$$\partial_t \varphi(\mathbf{r}, t) = \gamma \nabla^2 \frac{\delta \hat{F}}{\delta \varphi(\mathbf{r}, t)} - g \nabla \cdot \left[\varphi(\mathbf{r}, t) \frac{\delta \hat{F}}{\delta \mathbf{j}(\mathbf{r}, t)} \right] + \mu'(\mathbf{r}, t), \quad (2.21)$$

$$\begin{aligned} \partial_t j_i(\mathbf{r}, t) = & \frac{\eta}{\rho_0} \nabla^2 \frac{\delta \hat{F}}{\delta j_i(\mathbf{r}, t)} + \sum_k \frac{\sigma}{\rho_0} \nabla_i \nabla_k \frac{\delta \hat{F}}{\delta j_k(\mathbf{r}, t)} - g \varphi(\mathbf{r}, t) \nabla_i \frac{\delta \hat{F}}{\delta \varphi} \\ & - g \sum_k \left[\nabla_k j_i(\mathbf{r}, t) \frac{\delta \hat{F}}{\delta j_k(\mathbf{r}, t)} + j_k(\mathbf{r}, t) \nabla_i \frac{\delta \hat{F}}{\delta j_k(\mathbf{r}, t)} \right] + \nu'_i(\mathbf{r}, t), \end{aligned} \quad (2.22)$$

where the diffusion constant for the rescaled variables is defined, $\gamma = \Gamma K'$, the coupling parameter is now $g = \lambda(K/\rho_0)^{1/2}$, and μ' and ν' are the rescaled noise fields. We are still able to freely set the scale for the time and length,

$$\hat{l} = l\theta^{1/2}, \quad (2.23)$$

$$\tau = \gamma t. \quad (2.24)$$

We set the natural length scale $\theta^{-1/2}$ to unity,¹⁹ $\theta = 1$. We can then choose as our characteristic time γ^{-1} so that the time is given in dimensionless form in units of the diffusion time for the order parameter, $\tau = \gamma t$. For simplicity, we will continue to denote by \mathbf{r} the dimensionless coordinate. Our (2.14) and (2.15) now take the fully rescaled, dimensionless form,

$$\partial_t \varphi(\mathbf{r}, t) = \nabla^2 [\varphi^3(\mathbf{r}, t) - \varphi(\mathbf{r}, t) - \nabla^2 \varphi(\mathbf{r}, t)] - \hat{g} \nabla \cdot [\varphi(\mathbf{r}, t) \mathbf{j}(\mathbf{r}, t)] + \hat{\mu}(\mathbf{r}, t), \quad (2.25)$$

$$\begin{aligned} \partial_t j_i(\mathbf{r}, t) = & \hat{\eta} \nabla^2 j_i(\mathbf{r}, t) + \hat{\sigma} \sum_k \nabla_i \nabla_k j_k(\mathbf{r}, t) - \hat{g} \varphi(\mathbf{r}, t) \nabla_i [\varphi^3(\mathbf{r}, t) - \varphi(\mathbf{r}, t) - \nabla^2 \varphi(\mathbf{r}, t)] \\ & - \hat{g} \sum_k \{ \nabla_k [j_i(\mathbf{r}) j_k(\mathbf{r})] + j_k(\mathbf{r}) \nabla_i j_k(\mathbf{r}) \} + \hat{v}_i(\mathbf{r}, t). \end{aligned} \quad (2.26)$$

Here the transport coefficients are dimensionless and, at $\theta = 1$, they take the forms $\hat{\eta} = \eta / \rho_0 \gamma$, $\hat{\sigma} = \sigma / \rho_0 \gamma$. Also $\hat{g} = g / \gamma$. The noise sources have also been rescaled. They are given in terms of the original noise sources as

$$\hat{v}_i(\mathbf{r}, t) = \frac{1}{\Gamma} \left[\frac{u}{r \rho_0} \right]^{1/2} \left[\frac{1}{K'} \right]^{3/2} v_i(\mathbf{r}, t), \quad (2.27)$$

$$\hat{\mu}(\mathbf{r}, t) = \frac{1}{\Gamma K'} \left[\frac{u}{r} \right]^{1/2} \mu(\mathbf{r}, t). \quad (2.28)$$

Now the noise correlation functions in these rescaled equations are easily determined from the relations to the original noise sources and (2.16) and (2.17). We have the following correlations:

$$\begin{aligned} \langle \hat{v}_i(\mathbf{r}, \tau) \hat{v}_k(\mathbf{r}', \tau') \rangle \\ = -2\epsilon (\hat{\eta} \nabla^2 \delta_{i,k} + \hat{\sigma} \nabla_i \nabla_k) \delta^d(\mathbf{r} - \mathbf{r}') \delta(\tau - \tau'), \end{aligned} \quad (2.29)$$

$$\langle \hat{\mu}(\mathbf{r}, \tau) \hat{\mu}(\mathbf{r}', \tau') \rangle = -2\epsilon \nabla^2 \delta^d(\mathbf{r} - \mathbf{r}') \delta(\tau - \tau'), \quad (2.30)$$

where we have used the dimensionless temperature scale defined as

$$\epsilon = \frac{T}{K}. \quad (2.31)$$

Note that there are no cross correlations between the noise sources associated with the order parameter and with the currents while there are cross correlations between the noise sources associated with the different vector directions of the current. These cross correlations will complicate the procedure for generating the noise sources numerically.

The methodology of the solution of the above equations and the specific values of the parameters used are discussed in Sec. III.

III. METHODS

The general method we have used for solving the fundamental equations (2.25) and (2.26) follows the computational approaches that were developed in Refs. 7 and 20. We will discuss in this section only those portions of the procedure that are specific to the solution of this particular model. This model as written has four free parameters, $\hat{\eta}$, $\hat{\sigma}$, \hat{g} , and ϵ , whose possible values and effects in the calculation need now be discussed.

Previous computational studies of simpler models which neglected coupling to current fields showed that the depth of the temperature quench had no discernible influence on growth dynamics with the possible exception of a quench to zero temperature. The effect of the depth of the temperature quench has been studied experimentally in fluid systems. A dependence of the growth exponent n on the quench depth has been reported by some authors²¹ for binary fluid mixtures quenched to very near the critical point. In our opinion, a sufficiently deep quench is necessary to ensure that the system is in the unstable region where temperature plays little role in the growth of domains. Investigating a possible quench-depth dependence near the critical point in the growth behavior for fluid models would be a line of work worth pursuing in the future. Here, we will choose a small but nonzero temperature to which to quench, $\epsilon = 0.1$. It is important to note that the temperature in our calculations is set only through the value of the parameter ϵ which determines the noise correlation strength.²² The velocity correlations are not fixed as is the practice in molecular-dynamics simulations. At long times the current correlations must tend to the equilibrium value as given by the rescaled form of the equipartition theorem,

$$\langle j_i(\mathbf{r}) j_k(\mathbf{r}') \rangle_{\text{eq}} = \epsilon \delta_{ik} \delta(\mathbf{r} - \mathbf{r}'). \quad (3.1)$$

The coupling parameter \hat{g} is of considerable importance to this study of spinodal decomposition. When $\hat{g} = 0$, (2.25) decouples from (2.26) and becomes the equation for the scalar field in the standard model *B*.¹² Because the coupling to the currents greatly modifies the behavior of the field, the question of the crossover which must occur as \hat{g} increases from zero is of great interest. A study of this crossover phenomenon would require very great amounts of computer time and will not be pursued here. In this work we wish to consider, as stated in the introduction, the case where the coupling between order parameter and current is an important factor in the growth of ordered domains and we will therefore set $\hat{g} = 1$.

We have taken the dimensionless shear viscosity value to be $\hat{\eta} = 1$. This parameter (along with $\hat{\sigma}$) determines not only the relative weight of the noise strengths associated with the two dissipative mechanisms, as can be seen from (2.29) and (2.30), but also the relative diffusion times for the variables φ and \mathbf{j} [see (2.25) and (2.26)]. It seems

natural to take the relative weights of these noise strengths to be the same. Though the diffusion time of the order parameter and the dissipation time of the current field are taken to be the same, ordering the domains turns out to proceed more slowly than the current equilibrates. An interesting extension of this research would be to investigate the growth kinetics for a system in which the current dissipation time is markedly smaller. The value of the other viscosity $\hat{\sigma}$ is discussed below in connection with noise generation.

A very important additional parameter, implicit in Sec. II, is the dimensionality d . We have performed our calculations in two dimensions. We note here that the “universality” of the growth exponent n with respect to d has not been established for any Langevin model containing currents. Theoretical work^{8,9} appears to cast serious doubts upon this matter. We have studied this model only for a two-dimensional fluid which begs the question of the role dimensionality plays in the growth dynamics. In the future, it would be important to put this or other fluid models on a three-dimensional lattice and compare the dynamics. However, given the complexities of such models, a three-dimensional simulation would consume a larger amount of computer resources than is now available to us, and the exploration of the three-dimensional world will have to await further developments.

The coupled differential equations (2.25) and (2.26) are solved numerically by the Euler method: an iterative approximation for time integration. In this method, we define initial conditions for the dynamical variables, as discussed below, and evolve the system in time using these equations. These variables are evaluated at successive times by using their values at the previous time step. This solution was performed on a square two-dimensional lattice where periodic boundary conditions were used, and the differential operators were discretized in the usual way.

Next, the Gaussian noise sources $\hat{\mu}$ and $\hat{\nu}_i$ must be generated numerically, being careful to reproduce the proper correlations. Gaussian distributions can be obtained from a flat distribution such as the uniform computer-generated random numbers. As shown previously,²³ two Gaussian correlated fields are sufficient to generate the noise source $\hat{\mu}$ with the proper correlation. The noise fields $\hat{\nu}$ require the generation of six Gaussian fields in two dimensions in general but only four⁷ are needed in the particular cases where $\hat{\sigma}=0$ and $\hat{\sigma}=2$. Since the generation of the Gaussian fields is time consuming, the simplification associated with the use of these values is desirable. We have taken in this study $\hat{\sigma}=2$ which will preserve the coupling between the currents in the x and y directions.

It must be emphasized here that only one set of parameter values has been explored in this work. This raises the question of universality. We have seen that there is every expectation that there is no universality with respect to \hat{g} at least in the sense that the dynamics of this model with $\hat{g}=0$ should differ from nonzero \hat{g} . Regarding the remaining parameters nothing conclusive can be said at present. If there were a continuous change in the growth kinetics as the parameters are varied, universality

would be totally inapplicable to fluid models.

The initial conditions on the current and order parameter were designed to simulate a disordered state. The order parameter was at every lattice site set equal to zero, which is the condition of thorough mixing above T_c that we wish to simulate initially. This condition is intended to represent²⁴ a high-temperature situation where the free energy, (2.20), would be a single well centered about $\varphi=0$. The currents were given an initial Ising-like character. At each lattice site, j_x and j_y were initialized randomly to values of ± 0.1 with equal probability. The initial same site current correlation $\langle j_i j_i \rangle = 0.01$ corresponds to that for a very low temperature rather than the high-temperature state that we wish to simulate initially. But it was found that initial conditions on the currents were of little influence after relatively short times. The current correlations equilibrated quickly compared to the time scale of domain growth regardless of the initial conditions used. Since the variables in this simulation are coarse grained averages over volume elements, it is not unphysical to have a nonequilibrium state where the correlation strength of the average velocities within the volume elements are small.

The temperature quench is simulated by starting with the above-described initially distorted state and setting the noise correlation prefactor to the final temperature. This is an idealized fast-temperature quench in the sense that the temperature as measured by the noise fields is instantaneously changed. The response to this change is reflected in the dynamical variables.

In Sec. IV, we will use some terms that need to be defined here. We define a “run” as a single numerical solution to (2.25) and (2.26) beginning with one set of initial conditions. Our statistical quantities are obtained as an average over many such runs which amounts to an averaging over initial conditions and more significantly an average over the noise fluctuations. We found that large fluctuations can occur from run to run and that reliable statistics require averaging over a minimum of 20 runs, although nearly all of the results we present are averages over 55 to 100 runs. We used a “time step” $\Delta\tau=0.02$, after carefully verifying, by performing calculations in small systems, that this is a conservative estimate of the largest $\Delta\tau$ value which produces averaged results independent of $\Delta\tau$. Any quantity that we measure is obtained at selected times. We found that collecting the quantities necessary to perform the analysis in Sec. IV took a non-negligible amount of computer time, so that it was not possible to do our analysis at every time step.

The required lattice size $N \times N$ is determined by the initially unknown growth kinetics of this system in a trial and error method. It is a function of the maximum value τ_M of the time after the quench and it depends on the initially unknown growth law, since the characteristic domain size $l(\tau_M)$ must remain considerably smaller than the linear system size N . Given fixed computer resources τ_M and N must be determined in a self-consistent way. Beginning with relatively small lattices, we perform the calculations and the collection of the required information (to be described in more detail in Sec. IV) for a fixed

time range. If the size of the domains had grown to a significant fraction of the system size before the end of that time range, we then tried the same procedure on larger sizes, since results were in this case contaminated by finite-size effects. If, on the other hand, the results had proven free of finite-size effects, but did not exhibit the expected long-time behavior (i.e., a power-law growth, scaling) we then increased τ_M . This procedure establishes then, in an iterative manner, the optimum values of N and τ_M to be used. As we will see in Sec. IV, a size of $N=75$ allows for calculations of results free from finite-size effects to be obtained up to $\tau_M=370$ while $N=100$ is required for times to 470 and beyond. We will present evidence in Sec. IV that the latter value is within the scaling long-time regime. Note that, as N is increased, the absence or presence of finite-size effects was checked by comparing results for different sizes.

IV. RESULTS

The main objective of this research is to measure the growth of domains in our system as the numerical solution of (2.25) and (2.26) evolves through time. A naive method would be to look at "snapshots" of the two-dimensional lattice upon which is represented the value of the order parameter at each lattice site. The results of this method would be difficult to quantify, impossible to average in a meaningful way over multiple runs, and only useful as a qualitative check of the shape of the domains and the width of the domain boundaries. The best way to quantify the measure of domain growth as a function of time is to look at the equal time correlation functions, which can be easily averaged over runs, thus achieving in a practical way the averaging over noise and initial conditions with adequate statistics.

We have used two methods of analysis in this work in order to extract as much information as possible from the data. The first involves the collection and analysis of two-point correlation functions. From the point of view of order growth, the most important of these is the quasi-static two-point order-parameter correlation function $C(\mathbf{r}, \tau)$,

$$C(\mathbf{r}-\mathbf{r}', \tau) = \langle \varphi(\mathbf{r}, \tau) \varphi(\mathbf{r}', \tau) \rangle, \quad (4.1)$$

where \mathbf{r} and \mathbf{r}' are lattice vectors and $\langle \rangle$ indicate an average over the noise and initial conditions. Alternatively one can study the Fourier transform of this correlation function which is the quasistatic structure factor $C(\mathbf{k}, \tau)$,

$$C(\mathbf{k}, \tau) = \frac{1}{N^2} \sum_{\mathbf{r}, \mathbf{r}'} \exp[i\mathbf{k} \cdot (\mathbf{r} - \mathbf{r}')] \langle \varphi(\mathbf{r}, \tau) \varphi(\mathbf{r}', \tau) \rangle, \quad (4.2)$$

where the \mathbf{k} are the appropriate discrete set of vectors in the first Brillouin zone. It is sometimes numerically convenient to calculate $C(\mathbf{k}, \tau)$ directly as

$$C(\mathbf{k}, \tau) = \langle \varphi(\mathbf{k}, \tau) \varphi(-\mathbf{k}, \tau) \rangle, \quad (4.3)$$

where

$$\varphi(\mathbf{k}, \tau) = \frac{1}{N} \sum_{\mathbf{r}} \exp(i\mathbf{k} \cdot \mathbf{r}) \varphi(\mathbf{r}, \tau). \quad (4.4)$$

The Fourier transforms were efficiently performed using vectorized multidimensional fast-Fourier-transform routines available for the Cray 2. The correlation functions $C(\mathbf{r}, \tau)$ and $C(\mathbf{k}, \tau)$ not only provide measures of ordered domain size, but also of the scaling behavior and of the extent of the validity of our results near the time when they begin to be influenced by the finite size of our lattice.

We have also collected and studied the momentum density correlation functions defined as

$$C_{ik}(\mathbf{r}-\mathbf{r}') \equiv \langle j_i(\mathbf{r}, \tau) j_k(\mathbf{r}', \tau) \rangle \quad (4.5)$$

and the corresponding Fourier transforms. Though the momentum density does not order, the correlation functions C_{ii} are very useful in quantifying how the currents approach equilibrium. The conservation of momentum which prescribes that $C_{ii}(\mathbf{k}=0, \tau)$ is time independent prevents the $C_{ii}(\mathbf{k}, \tau)$ from evolving to a completely flat distribution, the Fourier transform of (3.1).

The correlation functions presented here were circularly averaged to remove the directional dependence of wave vector \mathbf{k} or lattice vector \mathbf{r} . The circular average for a continuous system would be performed by an angular integration. On a lattice, the circular averaging was performed by summing the correlation functions with arguments \mathbf{k} or \mathbf{r} which fall within a certain ring of width equal to the lattice spacing and then dividing by the number of sites in that range.

The other method that we used to measure the ordering evolution involves the calculation of the block correlation functions²⁵ $R_M(\tau)$ which are obtained by summing the order parameter over square blocks of a particular size $M \times M$ and averaging the square of this sum over multiple runs with a normalization as follows:

$$R_M(\tau) = \frac{1}{S(\tau)} \left\langle \left[\frac{1}{M^2} \sum_{\mathbf{R} \in M^2} \varphi(\mathbf{r}, \tau) \right]^2 \right\rangle, \quad (4.6)$$

where $S(\tau)$ is the average over the system of the square of the order parameter,

$$S(\tau) = \frac{1}{N^2} \sum_{\mathbf{r}} \langle \phi^2(\mathbf{r}, \tau) \rangle. \quad (4.7)$$

Some of the properties of $R_M(\tau)$ are obvious from looking at (4.6). The block correlation functions measure order over regions of size M . The quantity $R_M(\tau)$ is larger for smaller block sizes M . When $M \gg l(\tau)$ (the domain size at time τ), the sum over M extends over many domains of opposite signs and $R_M(\tau)$ is small. In the opposite limit, no such reduction occurs and $R_M(\tau)$ is larger.

We now begin a discussion of results by presenting some of the raw data obtained in our calculations. Figure 1 is a snapshot of the values of the order parameter at several specific times on the real-space lattice for one run. Examination of such snapshots for different runs shows that there is really no such thing as a "typical" run, therefore the reader is cautioned not to draw any excessively general conclusions from the particular shapes seen in this figure. The two earliest times pictured show an interwoven filamentary domain structure similar to that found for model *B* in Ref. 10. As we shall see, we find an

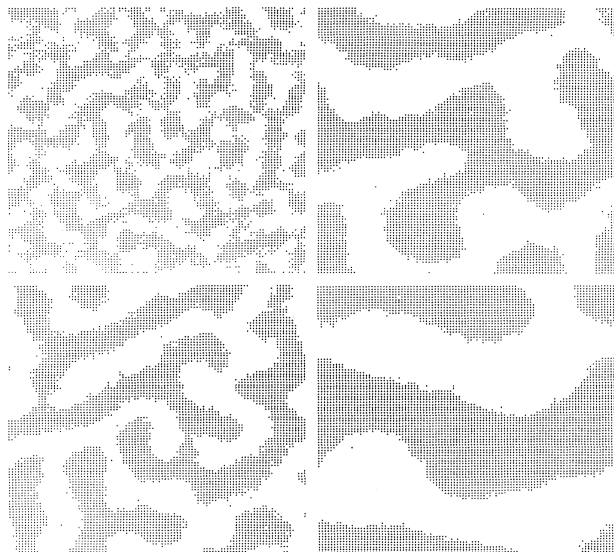


FIG. 1. In these four panels, we show “snapshots” of the domain structure for an $N=100$ system at four times, $\tau=25$, 100, 200, and 425 for one run. The sites with plus signs have a non-negative value of the order parameter. The first two times (pictured in the upper and lower left panels, respectively) correspond to the earlier-time regime discussed in the text. The upper and lower right panels are at $\tau=200$ and 425, respectively. At late times, the domain shape is very variable from run to run. Sometimes there are strips as pictured here; in other runs, the domains are more circular. We typically have 4–6 domains toward the end of our runs.

effective exponent $n \sim 0.3$ in this range. Later, there is a crossover to faster growth. This time range is displayed in the last two panels. The domain boundaries have a width of only a few lattice spacings which is not evident from this type of picture. Note that the conservation law appears to be obeyed limiting $\langle \varphi \rangle_{\text{system}} = 0$, the initial average value of the order parameter. The shape of the domains is irregular, but does not appear to be dictated by the geometry of the underlying lattice. At time $\tau=425$, we have, as we shall see, a domain size approximately equal to 18 averaged over all runs. As can be seen from this figure no quantitative measure of domain size can be obtained without further analysis. More quantitative measures are obtained from the correlation functions.

In Fig. 2 we show, at early times, the circularly averaged correlation function $C(k, \tau)$ which is proportional to the experimentally measured light scattering intensity.^{4,5} The growth of order can clearly be seen. Note that the peak grows higher with increasing time and that its location moves toward smaller k . The peak position k_{max} is a measure of the characteristic length $l(\tau) \sim 1/k_{\text{max}}$. One more necessary check of our calculation can be made from Fig. 2, namely, that the order parameter is conserved as expected. $C(k=0, \tau)$ is the sum of the order-

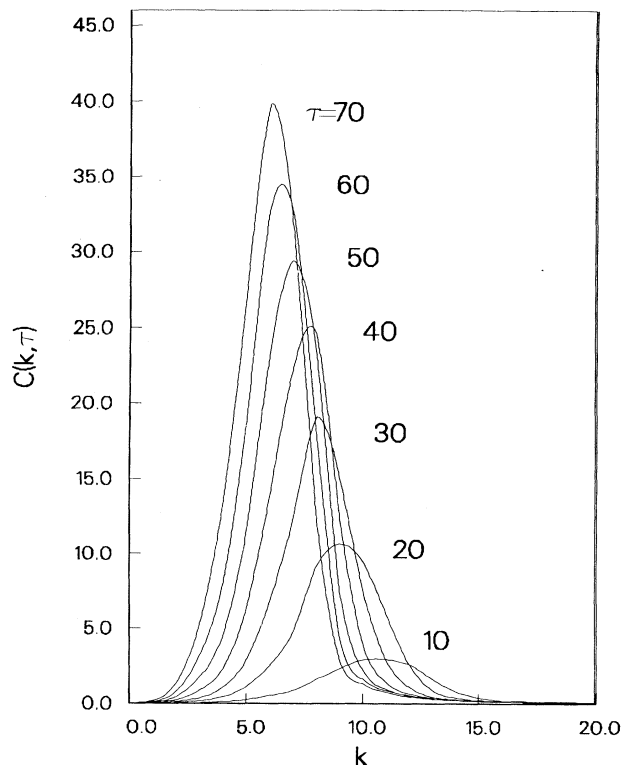


FIG. 2. Quasistatic structure factor $C(k, \tau)$ shown for several early and intermediate times for $N=100$ size systems averaged over 30 runs. The smooth curves are third-order polynomial interpolations to the data measured at discrete values of k . The k values are normalized by $N/2\pi$.

parameter correlations over the entire system. Since this quantity was initially zero, it should be zero for all times. At the longest times studied, as the peak position moves toward $k=0$, $C(k=0, \tau)$ remains less than 10^{-6} , a quantity numerically quite acceptable as zero in this calculation as compared to the height of the peak. This method of analysis of $l(\tau)$ in terms of $k_{\text{max}}(\tau)$ is not convenient at later times because of increasing uncertainties in determining the precise position of the maximum $k_{\text{max}}(\tau)$, which is difficult to interpolate since the maximum is sharp and the lattice resolution is coarse. The results in Fig. 2 are for a 30-run average on a $N=100$ lattice.

A more convenient measure of domain growth can be obtained from the real-space correlation function.²⁶ In Fig. 3 we show the raw data for the circularly averaged real-space correlation function $C(r, \tau)$. This correlation function was obtained by first Fourier transforming the two-dimensional correlation function $C(\mathbf{k}, \tau)$ and then performing the circular average. The plotted results represent averages over 55 runs ($N=100$). Note that for later times the system is becoming more ordered as the peak $C(r=0, \tau)$ becomes higher at later times and the first zero occurs at larger distances; the spreading of the distribution is an indication that the domains are growing larger. Any measure of the width of this distribution in-

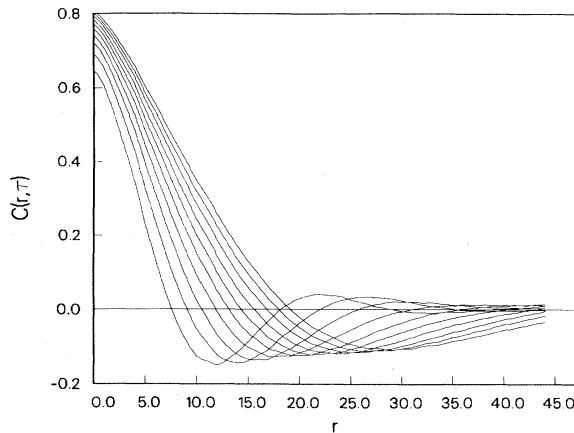


FIG. 3. Order-parameter correlation function $C(r, \tau)$ plotted for several times: $\tau=100, 130, 160, 210, 270, 330, 390,$ and 450 , respectively, from left to right at zero crossing, for a size $N=100$ system averaged over 55 runs. Increasing order is measured by the spreading width of the distribution which is a direct result of increasing domain size.

creases at later times. We will choose the position $r_0(\tau)$, of the first zero of $C(r, \tau)$ as a measure of $l(\tau)$ and will later show that all lengths are evolving in the same manner. Analyzing domain size in terms of $r_0(\tau)$ has none of the finite resolution effects encountered at long times in the analysis of the $1/k_{\max}$.

Let us consider now the block correlation functions. In Fig. 4 is plotted the raw data of $R_M(\tau)$ versus τ for several values of M . Order as measured by this quantify is obviously increasing with time. Note that $R_M(\tau)$ is a decreasing function of M as expected since the ordered regions are at these times a small fraction of the larger block sizes. In this scheme one calculates block correlation functions for many block sizes, and so one can better quantify the measure of the scaling regime as discussed later. The results shown in this figure are for a 75×75 system. Values of $R_M(\tau)$ were calculated for all M in the range $25 \leq M \leq 42$, but for the sake of clarity, only every third M value is shown in the figure.

Results for the structure factor were obtained both for $N=75$ (100 runs) and $N=100$ (55 runs) systems. Comparison of these results show that finite-size effects begin in the 75×75 system at $\tau \sim 350$, which is why later times are not shown in Fig. 4. It will be seen later that the domain size at $\tau=350$ is $l(\tau) \sim (0.2) \times 75$. In our preliminary runs at smaller sizes, results for both block-correlation functions and two point-correlation functions have consistently given evidence of a threshold for finite-size effects at $l(\tau) \sim 0.2N$. This is also the case for other models. For $N=100$, this limit is reached at $\tau \sim 500$. Thus we are confident that results such as those in Figs. 3 and 4 are free from finite-size problems.

We now begin the analysis of our data by presenting the real-space current-current correlation function and its Fourier transform which are shown in Figs. 5 and 6

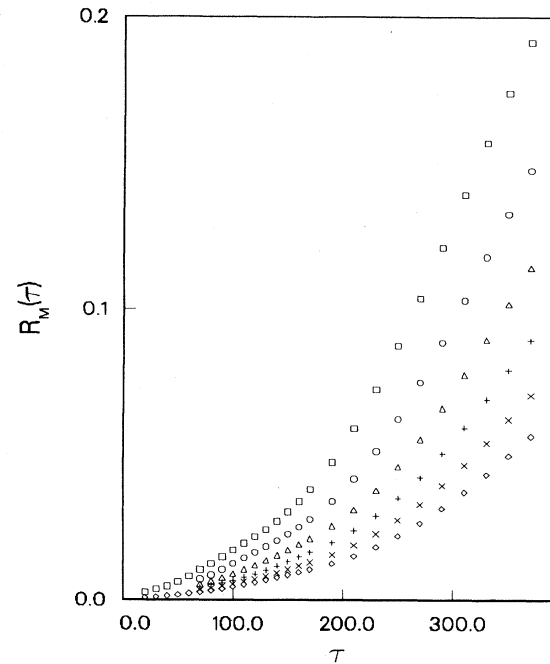


FIG. 4. Block correlation function results for selected block sizes are plotted vs time. Results are plotted for size $N=75$ averaged over 100 runs. Results were obtained for all M in the range $25 \leq M \leq 42$, but the values shown are from, top to bottom, $M=27, 30, 33, 36, 39,$ and 42 .

averaged over 55 runs ($N=100$) for several times. It is evident from the plots that the current equilibrates much faster than the domains order. The form of the equilibrated currents is approximately uncorrelated as expected from the equipartition theorem. Thus in Fig. 5 the real-space correlation function $C_{xx}(r, \tau)$ is very nearly a Kronecker δ , the strength of which is close to the equilibrium value $C_{xx}(r=0, \tau) = \epsilon$ but with a small width of $r \cong 2$. The current correlations cannot quite reach equilibrium due to the conservation of total momentum which constrains $C_{ii}(\mathbf{k}=0, \tau)$ to its initial value, equal to 0.01 with our initial conditions; however, for larger k they very quickly reach a time-independent value as close to equilibrium as this constraint allows. This is also shown in \mathbf{k} space in Fig. 6. We see that for a wide range of k values, $C(k, \tau)$ is very close to being a constant in k and τ for all times, $\tau \geq 10$. There is however a slight decrease in $C_{ii}(k, \tau)$ with increasing k . This near agreement with the expected form of the current correlations in equilibrium may be somewhat surprising since throughout this calculation the structure factor is far from equilibrium. The currents reflect the temperature of the heat bath represented by the noise correlation strength.

We proceed now to the characterization of domain growth, which must be studied in terms of the density correlations. We have used two measures of the domain size $l(\tau)$. One measure is $r_0(\tau)$, the first zero of $C(r, \tau)$. The other will be defined below in terms of the block

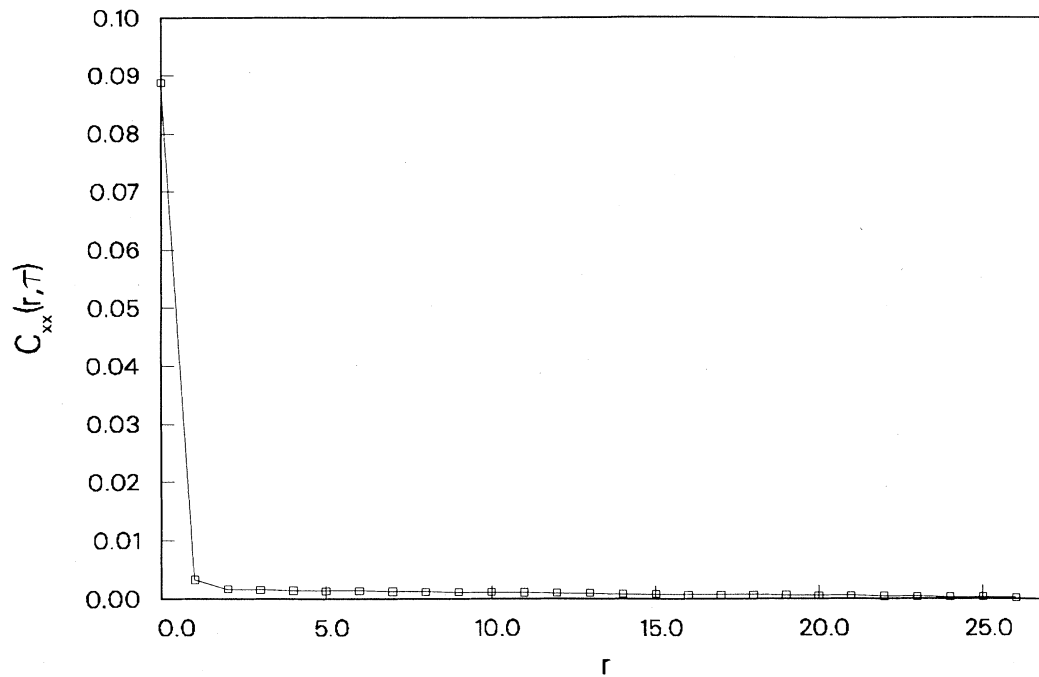


FIG. 5. Current-current correlation function $C_{ii}(r, \tau)$ plotted vs r at time $\tau=470$. Results shown are a 55-run average for $N=100$. Results for other times, $\tau \geq 10$, are nearly identical, and if plotted here would appear virtually superimposed to those shown. One sees that this result is very close to the equilibrium Kronecker δ .

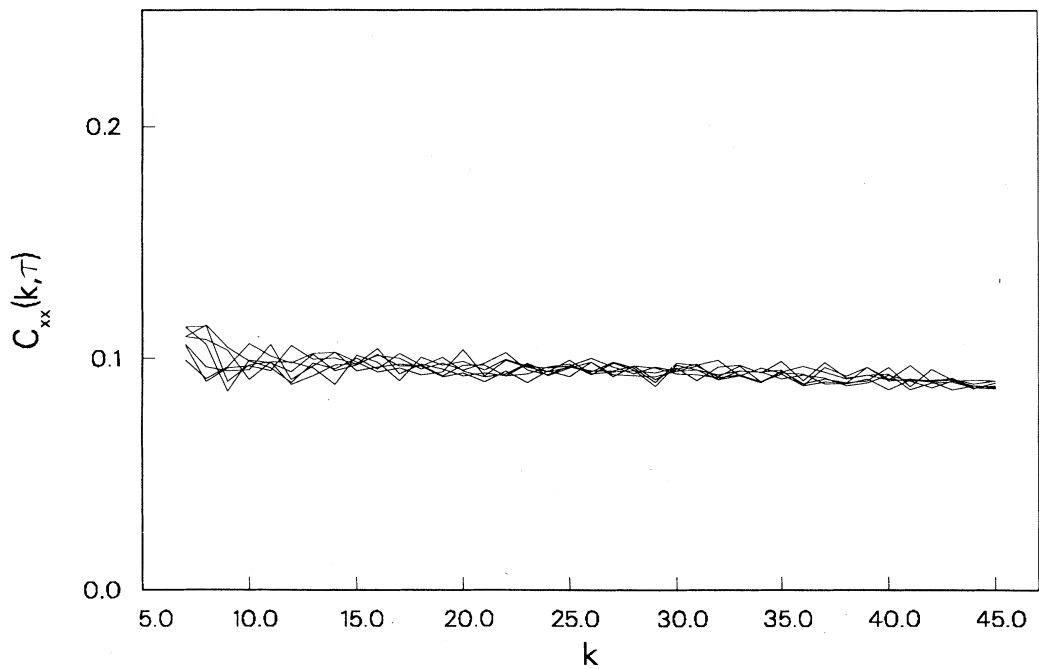


FIG. 6. Current-current correlations $C_{ii}(k, \tau)$ in k space are pictured here for several times $10 \leq \tau \leq 70$ showing the quick equilibration of this quantity within statistical error. At these and later times, $C_{ii}(k, \tau)$ is nearly independent of k and τ . The k values are normalized as in Fig. 2.

correlations. It has been observed both experimentally and numerically for a variety of systems and models that, at sufficiently long times, the distribution functions which measure the domain growth exhibit scaling behavior. In that case it does not matter which measure of domain size is taken. In this work we will show that our two measures coincide even at relatively early times.

For the first measure we investigate the block correlation functions $R_M(\tau)$. To extract a characteristic length from these functions, we use the fact that in the scaling regime we must have

$$R_M(\tau) = g \left[\frac{L(\tau)}{M} \right] \equiv g(y), \quad (4.8)$$

where the length $L(\tau)$ is a measure of domain size. The scaling function for systems with conserved order parameter can be shown to be of the form²⁷ $g(y) = y^3$ for small y . We therefore have

$$R_M(\tau) = \left[\frac{L(\tau)}{M} \right]^3 \left[1 + O \left(\frac{L(\tau)}{M} \right) \right]. \quad (4.9)$$

In Fig. 7 we have plotted the quantity $R_M^{1/3}(\tau)M$ versus M at several times. We find that the quantity plotted is,

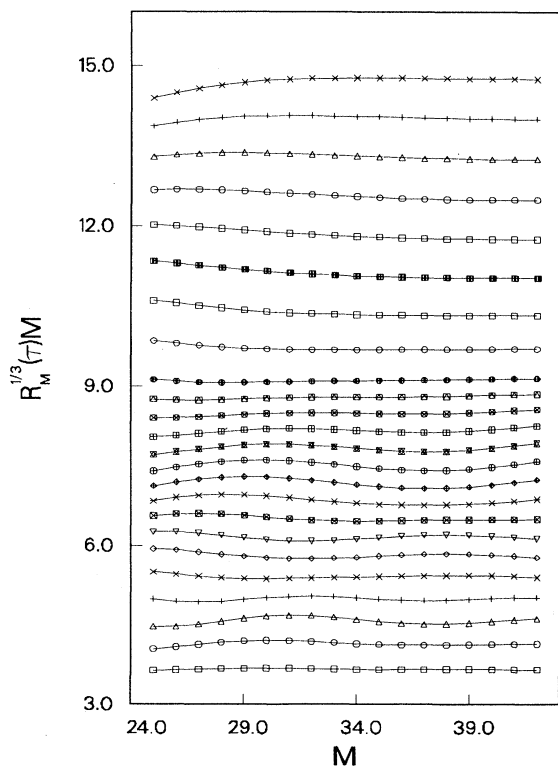


FIG. 7. Quantity $R_M^{1/3}(\tau)M$ plotted as a function of M for times $\tau=20$ to 330. The time interval is $\Delta\tau=10$ up to $\tau=170$ and $\Delta\tau=20$ thereafter, from bottom to top. In this range this quantity is, within statistical uncertainty, independent of M . The system size and number of runs are as in Fig. 4.

within statistical error, independent of M . The fluctuations are consistent with the statistical uncertainty of our results. According to (4.8) and (4.9) this means that we have found scaling behavior for $R_M(\tau)$ and that $g(y) \approx y^3$ in the time range plotted. Note that the behavior of $g(y)$ is different from that of Ref. 7, where a y^4 correction was evident. This particular scaling behavior implies that we can define a characteristic length from the block correlation functions as

$$L(\tau) = \langle R_M^{1/3}(\tau)M \rangle_M, \quad (4.10)$$

where $\langle \rangle_M$ indicates in this equation an average over results at each block size. This length will be compared with r_0 as a further verification of scaling behavior.

In Fig. 8 we compare our two measures of domain size. Both $L(\tau)$ and $r_0(\tau)$ are plotted versus time; all data were obtained from the same 100 runs on an $N=75$ lattice. For times $\tau < 370$, not only do the two measures of $l(\tau)$ exhibit the same time dependence, but also they numerically coincide. No adjusting scale factor has been used. That two disparate measures of domain size should be related by a constant of proportionality is a test of scaling. The fact that the constant of proportionality is unity is a happenstance that we have yet to explain. We have chosen to show in this figure the finite-size effects which occur at this value of N for times $\tau > 370$. In this range, the plots for r_0 and L begin to diverge from each other. Here the characteristic size of the domains is approximately 15 or larger. This equals or exceeds 20% of the system size and, therefore, finite-size effects are significantly influencing our results in different ways causing these two measures to deviate from each other.

In the scaling regime, $C(r, \tau)$ should be characterized by a scaling function $f(x)$,

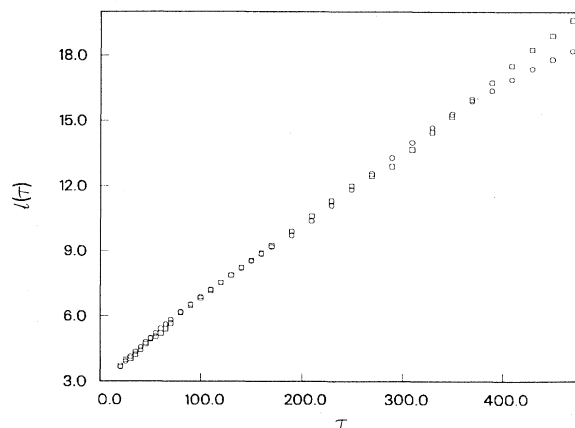


FIG. 8. A comparison as a function of time of the two lengths $r_0(\tau)$ (circles) and $L(\tau)$ (squares) which we take as measures of the domain size $l(\tau)$. The results plotted are averages over the same 100 run for an $N=75$ system. The two lengths are not only proportional to each other, but also identical up to the onset of finite-size effects (see text) at $\tau \approx 370$.

$$C(r, \tau) = f(r/r_0(\tau)) \equiv f(x). \quad (4.11)$$

Thus in this regime $C(r/r_0(\tau), \tau)$ should be a function only of the quantity $x = r/r_0(\tau)$ except at very small r , where scaling never holds. To check this hypothesis, we have plotted in Fig. 9, $C(x, \tau)$ versus x for several times using our results for 55 runs at the largest sizes ($N = 100$) and the longest times (up to $\tau_M = 470$) that we have studied. We find that scaling for $C(x, \tau)$ is obeyed for times greater than $\tau \approx 200$.

In Fig. 10 we have made a comparison of the scaled correlation function $f(x)$ with the scaling function obtained for model *B* in Ref. 10. One can clearly see that the two scaling functions are different. However, we have plotted also in this figure some of our data at earlier times, before scaling is reached. This data turns out to correspond reasonably well to the scaling function from model *B* for larger r . The second zeros for both our early time data and model *B* are the same and the first minimum and second maximum are in fair agreement both in location and in magnitude. At small r , our early-time data fall short of the $r = 0$ peak, which is an indication that the local value of the order parameter has not yet reached its equilibrium value. For model *B* at early times, there is a similar tendency for the peak at $r = 0$ to be lower than the peak is in the scaling regime.

We can also analyze the behavior of the domain size as a function of time. It is obviously important to do that at the longest time ranges reached. Expecting power-law growth, we have plotted in Fig. 11 the size $r_0(\tau)$ versus time on a log-log scale. For times up to 370, we have plotted the properly weighted averages of our $N = 75$ and $N = 100$ results, and for later times, only the $N = 100$ results. We performed a least-squares fit to a power-law form, $l(\tau) = A\tau^n$, for late-time data $150 \leq \tau \leq 470$. We obtained a growth exponent $n = 0.69 \pm 0.02$. This fit is

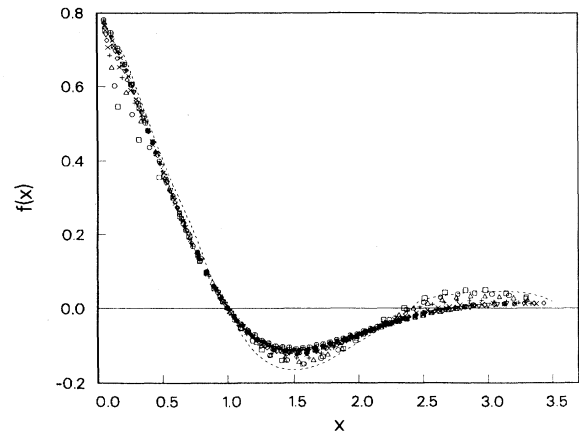


FIG. 10. A comparison between the scaling function for model *B* and the scaled correlation function $C(r, \tau)$ obtained for the model studied here. The dashed line represents the late-time scaling function for model *B* from Ref. 10. The symbols are data from our calculations for times $80 \leq \tau \leq 470$. The earliest-time data pictured, $\tau = 80$ (squares) and $\tau = 100$ (circles), are in fairly good agreement with the scaling function for model *B*, while the later-time results, which represent the scaling function shown in Fig. 9, are different (see text).

represented by a dashed line in Fig. 11. At much earlier times, there seems to be a regime with exponent $n \approx 0.3$, consistent with model-*B* values. The influence of currents is responsible for a crossover to a substantially faster growth process. The existence of two regimes is in good agreement with what is experimentally found for real fluids, as explained in Sec. I.

It should be emphasized that this measured growth exponent cannot be conclusively taken to be the confirmed

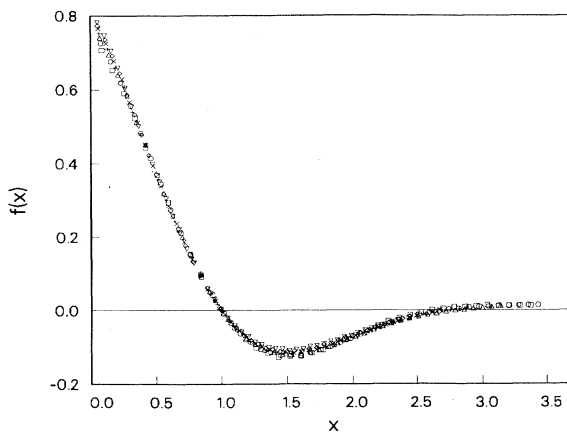


FIG. 9. Scaling function $f(x)$ for $C(r, \tau)$ obtained from the same runs as in Fig. 3 as a function of $x = r/r_0(\tau)$. The times plotted are $230 \leq \tau \leq 470$ for intervals of $\Delta\tau = 40$. For these times, the curves are within statistical error the same: the scaling function for the fluid model studied here.

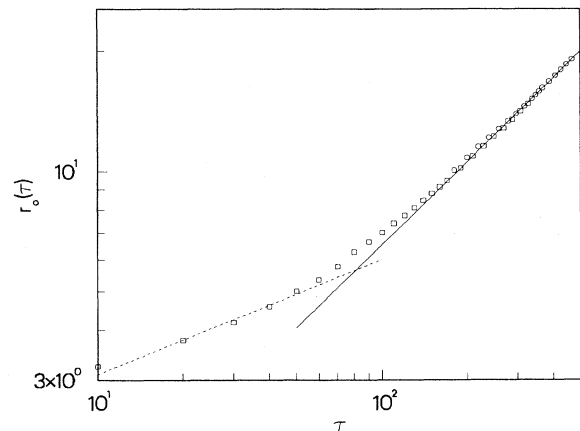


FIG. 11. Plot of the domain size as measured by $r_0(\tau)$. The squares are data obtained by taking the weighted average of 55 runs at $N = 100$ and 100 runs at $N = 75$. The circles are data only from the $N = 100$ system. The best power-law fit to the data for $\tau \geq 150$ is also shown as the solid line. It corresponds to an exponent of $n = 0.69 \pm 0.02$. At earlier times, a regime with an effective exponent $n \approx 0.3$ (dashed line) is noted.

asymptotic value since one might question whether we have run our calculation long enough to confirm a power-law behavior. It has been argued in Ref. 10 that times at least of order ~ 1000 (in our units) are required in certain cases to attain the asymptotic region for model *B*. We have not run our calculations to these time scales but we have reached larger domain sizes than those in Ref. 10. The fact that the exponent we find is larger makes the present model much more difficult to study, since increased system sizes are needed. However, a calculation of an effective $n(\tau)$ exponent does not show any clear tendency to increase with time at later times. An increase of n to the value $n=1$ found for three-dimensional fluids seems to be unlikely from an analysis of our data. The asymptotic value of n could be dimensionally dependent.⁹ We believe that our results are strong, although not conclusive evidence for an asymptotic value of $n \approx 0.7$ for this model. In any event, our data leave no doubt that the late-time exponent for this model is not only considerably larger than that observed for model *B*, but also larger than the value $n = \frac{1}{2}$ reported in Ref. 7 for a different fluid model, thus showing that heat transport is quite relevant in spinodal decomposition.

Thus we have shown in this calculation that the form of the coupling of the order parameter to the current

makes a significant difference in the growth of domains in SD. Diffusive dynamics promotes faster domain growth than do oscillatory pressure fluctuations in the later stages of growth.

The question of universality classes for fluid systems has been challenged here. Our results imply that not all two-dimensional fluid models are in the same universality class. Also, there is the possibility that continuous adjustments of the coupling parameter may lead to a continuous change in the growth behavior. We have only checked one point in parameter space. Since \hat{g} is clearly relevant, other parameters might also be. Between $\hat{g}=0$ and $\hat{g}=1$ there is a transition between the slower dynamics of model *B* and the faster dynamics measured here. The exact nature of that transition will determine whether universality classes can be assigned to fluid systems. Very likely, at any finite \hat{g} there is a crossover to a faster value of n . The time of this crossover will clearly depend on \hat{g} , but we cannot tell whether the asymptotic value also depends on \hat{g} . Investigating these questions must be left to future research.

ACKNOWLEDGMENTS

This work was supported in part by the Minnesota Supercomputer Institute and the University of Minnesota Graduate School Research Fund.

- ¹For reviews of the subject see K. Binder, in *Systems Far from Equilibrium*, Vol. 132 of *Lectures Notes in Physics*, edited by L. Garrido (Springer-Verlag, Berlin, 1980); J. D. Gunton and M. Droz, in *Introduction to the Theory of Metastable and Unstable States*, Vol. 183 of *Lecture Notes in Physics*, edited by J. Zittartz (Springer-Verlag, Berlin, 1983); K. Binder, *Physica A* **140**, 35 (1986).
- ²T. Hashimoto, K. Nishimura, and Y. Takeuchi, *Phys. Lett.* **65A**, 250 (1978); M. Hennion, D. Ronzaud, and P. Guyot, *Acta. Metall.* **30**, 599 (1982); S. Katano and M. Iizumi, *Phys. Rev. Lett.* **52**, 835 (1984).
- ³S. Komura, K. Osamura, H. Fujii, and H. Takeda, *Phys. Rev. B* **31**, 1278 (1985).
- ⁴N. Wong and C. Knobler, *J. Chem. Phys.* **69**, 725 (1978); *Phys. Rev. A* **24**, 3205 (1981); E. Siebert and C. Knobler, *Phys. Rev. Lett.* **54**, 819 (1985).
- ⁵Y. C. Chou and W. I. Goldberg, *Phys. Rev. A* **20**, 2015 (1979); A. J. Schwartz, J. S. Huang, and W. I. Goldberg, *J. Chem. Phys.* **62**, 1847 (1975); **63**, 599 (1975).
- ⁶K. Binder and D. W. Heermann, in *Scaling Phenomena in Disordered Systems*, edited by R. Pym and A. Skjeltrop (Plenum, New York, 1985); H. Furukawa, *Adv. Phys.* **34**, 703 (1973); J. D. Gunton, in *Time Dependent Effects in Disordered Materials*, edited by R. Dynn (Plenum, New York, 1987); Z. W. Lai, G. F. Mazenko, and O. T. Valls, *Phys. Rev. B* **37**, 9481 (1988).
- ⁷O. T. Valls and G. F. Mazenko, *Phys. Rev. B* **38**, 11 643 (1988).
- ⁸E. Siggia, *Phys. Rev. A* **20**, 595 (1979).
- ⁹M. San Miguel, M. Grant, and J. D. Gunton, *Phys. Rev. A* **31**, 1001 (1985).
- ¹⁰T. M. Rogers, K. R. Elder, and R. C. Desai, *Phys. Rev. B* **37**, 9638 (1988).
- ¹¹O. T. Valls and G. F. Mazenko, *Phys. Rev. B* **38**, 11 650 (1988); E. T. Gawlinski, J. Viñals, and J. D. Gunton, *Phys. Rev. B* **39**, 7266 (1989).
- ¹²P. C. Hohenberg and B. I. Halperin, *Rev. Mod. Phys.* **49**, 435 (1977).
- ¹³Although $n \approx 0.3$ is quoted specifically for model *B*, other diffusion-limited growth studies have found similar results, such as studies of spin-exchange Ising models; see, for example, D. A. Huse, *Phys. Rev. B* **34**, 7845 (1986).
- ¹⁴K. Kawasaki, *Ann. Phys. (N.Y.)* **61**, 1 (1970), and references therein.
- ¹⁵D. Forster, *Hydrodynamic Fluctuations, Broken Symmetry, and Correlation Functions* (Benjamin, New York, 1975), Chap. 4.
- ¹⁶This variable is a measure of the entropy density. Its precise definition is in Eq. (5.2) of Ref. 12.
- ¹⁷H. Mori and H. Fujisaka, *Prog. Theor. Phys.* **49**, 764 (1973); H. Mori, H. Fujisaka, and H. Shigematsu, *ibid.* **51**, 109 (1974).
- ¹⁸In the equilibrium ordered phase, the longitudinal current leads to a second-sound normal mode which, in the non-equilibrium regime studied here, would not propagate across domain walls.
- ¹⁹When numerically solving the problem on a lattice, this is
- ²⁰O. T. Valls and G. F. Mazenko, *Phys. Rev. B* **34**, 7941 (1986).
- ²¹E. Siebert and C. Knobler, Ref. 4.
- ²²In some studies of model *B*, the parameter ϵ is defined as being our 2ϵ .
- ²³R. Petschek and H. Metiu, *J. Chem. Phys.* **79**, 3443 (1985).
- ²⁴A physically better, but numerically awkward initial condition for the order parameter would be a broad Gaussian distribution of values centered about the origin.
- ²⁵More details on block correlations are given in Ref. 11.
- ²⁶We also tried using the first moment of $C(\mathbf{k}, \tau)$, but this quantity is affected by statistical fluctuations at large values of k .
- ²⁷This is proved in Appendix A of Ref. 11.